ACS OMEGA

Open Access

http://pubs.acs.org/journal/acsodf

Article

Hedgehog Zinc Oxide–Graphene Quantum Dot Heterostructures as Photocatalysts for Visible-Light-Driven Water Splitting

Thi Kieu Oanh Le,[#] Mitesh Ganpat Mapari,[#] and TaeYoung Kim*

Cite This: *ACS Omega* 2024, 9, 40790–40800

Read Online

ACCESS | Metrics & More | Article Recommendations | Supporting Information

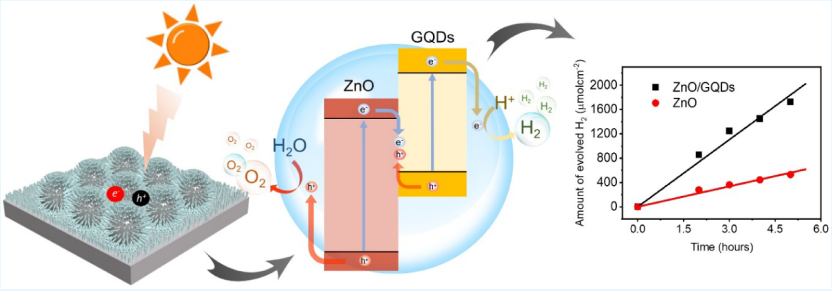

ABSTRACT: The development of efficient photocatalysts for sustainable hydrogen production via water splitting is vital for advancing renewable energy technologies. In this study, we present the synthesis and characterization of a novel visible-light-active photocatalyst comprising hedgehog-shaped zinc oxide (ZnO) nanostructures coupled with graphene quantum dots (GQDs). Optical properties assessed by UV–visible and photoluminescence (PL) spectroscopy revealed that the ZnO/GQDs heterostructure possessed a reduced band gap (2.86 eV) compared with pristine ZnO (3.10 eV), resulting in improved light absorption and charge separation. Electrochemical analyses indicated a significantly higher photocurrent response and lower charge transfer resistance for the ZnO/GQDs heterostructure compared with the pristine ZnO nanostructure. Photocatalytic tests demonstrated that the ZnO/GQDs heterostructure achieved over 3-fold higher hydrogen (H_2) production rates, with an apparent quantum yield (AQY) of 1.51% at 440 nm, and maintained stable activity over prolonged reaction periods. These results highlight the enhanced photocatalytic efficiency and stability of the ZnO/GQDs heterostructure, underscoring its potential as a high-performance photocatalyst for sustainable hydrogen generation. The synergistic effects between ZnO nanostructures and GQDs offer valuable insights into the design of advanced photocatalytic materials for renewable energy applications.

1. INTRODUCTION

Photocatalysis has emerged as a promising avenue for sustainable energy production by harnessing solar energy for chemical reactions, notably water splitting for hydrogen generation.[1,2] Semiconductor photocatalysts, such as metal oxides and sulfides, including titanium dioxide (TiO_2), zinc oxide (ZnO), tungsten trioxide (WO_3), tantalum pentoxide (Ta_2O_5), cadmium sulfide (CdS), and zinc sulfide (ZnS), have attracted significant attention due to their ability to directly utilize sunlight to activate the catalysts, along with their stability and abundance.[1−6]

However, these single-component semiconductor photocatalysts face challenges that hinder their practical application. Their wide bandgaps lead to inefficient utilization of solar irradiation, leaving the majority of photons in the visible spectrum unused and limiting their quantum yield. Additionally, the rapid recombination of photogenerated charge carriers curtails charge separation and transfer efficiency, resulting in low overall photocatalytic activity.[5,7]

To address these challenges, various strategies have been proposed to enhance the efficiency of photocatalysts for water splitting. These strategies include designing and synthesizing heterostructured photocatalysts by integrating different semiconducting materials to create favorable charge transfer pathways and improve light absorption properties.[8−11] Another approach involves modifying photocatalyst surfaces through the deposition of cocatalysts or sensitizing agents, such as noble metal nanoparticles or organic dyes, to facilitate charge separation and promote specific reaction pathways.[9,12−14] Additionally, engineering the morphology and nanostructure of photocatalyst materials has been explored to enhance light-harvesting efficiency, increase surface area, and promote charge carrier mobility.[15,16] Beyond these strategies, the introduction of homojunctions can facilitate the spatial separation of photogenerated electron–hole pairs, leading to enhanced charge

Received: June 14, 2024
Revised: July 29, 2024
Accepted: September 5, 2024
Published: September 16, 2024

Scheme 1. (a,b) Illustration of the Synthesis Method for the ZnO Hedgehog-Shaped (HGs) Substrate and (c) Illustration of ZnO Functionalized with Graphene Quantum Dots (GQDs) (ZnO/GQDs)

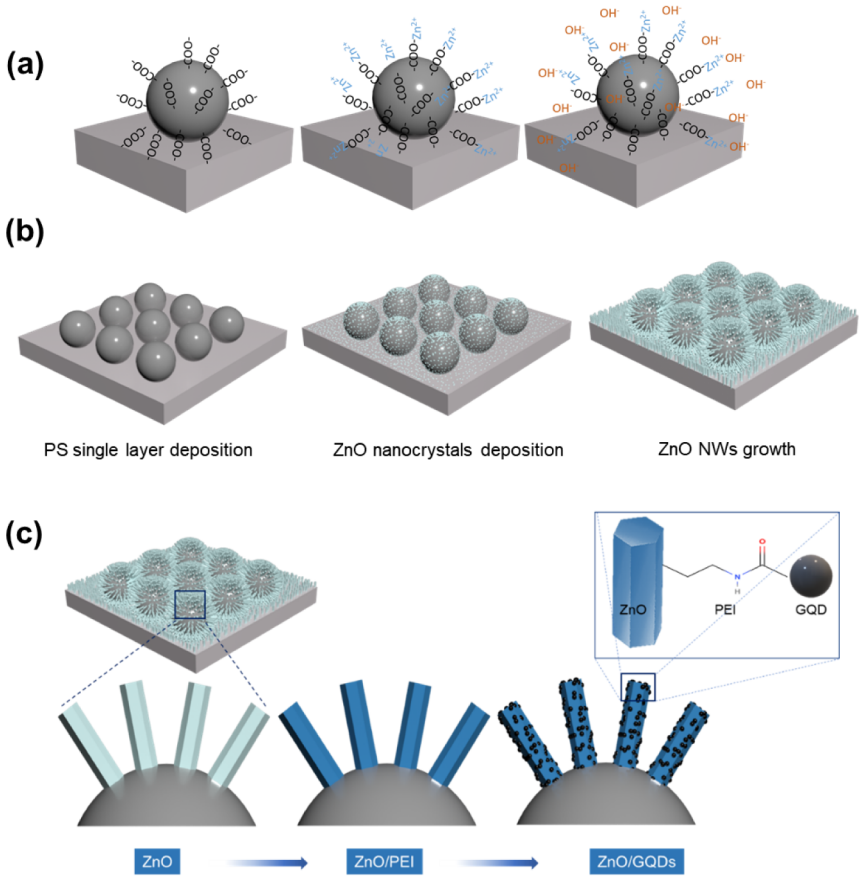

transport and increased availability of reactive species for catalytic reactions.[17] Furthermore, the reverse barrier layer concept has been investigated as a strategy to suppress the recombination of photogenerated charge carriers, promoting their participation in the desired catalytic processes and improving the overall photocatalytic performance.[18]

In this context, integrating graphene quantum dots (GQDs) with ZnO nanostructures presents a compelling strategy to synergistically enhance the photocatalytic activity for water splitting. GQDs, with their unique electronic and optical properties, offer excellent potential for extending the light absorption range to the visible spectrum and facilitating efficient charge separation and transfer dynamics.[19−21] Meanwhile, ZnO nanostructures, characterized by their high surface area-to-volume ratio and intrinsic photocatalytic activity, serve as ideal platforms for anchoring GQDs and promoting interfacial charge transfer processes. The heterostructure formed by coupling ZnO nanostructures with GQDs not only extends the light absorption range but also mitigates the recombination of photogenerated charge carriers, thereby enhancing the overall efficiency of water splitting and hydrogen production. Moreover, the tunability of GQDs allows precise control over the band alignment at the heterojunction interface, further optimizing charge transfer kinetics and photocatalytic performance.[20,22]

Furthermore, the utilization of spiky, hedgehog-shaped ZnO nanostructures offers unique benefits for photocatalytic applications. These hierarchical nanostructures provide increased surface area and multiple light-scattering sites, facilitating enhanced light absorption and efficient utilization of incident photons. Additionally, the spiky morphology promotes rapid charge transport and diffusion, minimizing charge recombination and enhancing photocatalytic activity.[23] The matching of energy band edges between zinc oxide and graphene quantum dots in the heterostructure configuration not only facilitates efficient charge separation and transfer but also holds the potential to enable S-scheme charge transfer pathways. The establishment of an S-scheme mechanism can further enhance the overall efficiency of water splitting by prolonging the lifetime of photogenerated charge carriers and promoting redox reactions at distinct sites within the photocatalyst.[21]

In this article, we present an investigation into the synthesis, characterization, and photocatalytic performance of hedgehog-like ZnO nanostructures coupled with graphene quantum dots as visible-light-active photocatalysts for water splitting. Through a systematic analysis of the structural, optical, and electrochemical properties, we elucidate the mechanisms underlying the enhanced photocatalytic activity and provide insights into the design principles for next-generation photocatalysts aimed at sustainable energy production.

2. EXPERIMENTAL SECTION

2.1. Chemicals. For the synthesis of ZnO nanostructures, zinc acetate dihydrate ($Zn(CH_3COO)_2{\cdot}2H_2O$), zinc nitrate hexahydrate ($Zn(NO_3)_2{\cdot}6H_2O$), and hexamethylenetetramine (HMTA, $C_6H_{12}N_4$) were purchased from Sigma-Aldrich (Korea). Polystyrene (PS) microspheres with an average size of 3.5 μm were purchased from SOKEN Chemicals (Japan). For the synthesis of GQDs, glucose ($C_6H_{12}O_6$), ammonium

https://doi.org/10.1021/acsomega.4c05574
ACS Omega 2024, 9, 40790−40800

chloride (NH_4Cl), potassium hydroxide (KOH), sulfuric acid (H_2SO_4), and nitric acid (HNO_3) were purchased from Sigma-Aldrich (South Korea). Deionized water (DI water) was used throughout the experiments.

2.2. Synthesis of Hedgehog ZnO Nanostructures. The synthesis of hedgehog-shaped ZnO nanostructures involved the following steps (Scheme 1a,b): (i) preparation of a PS microsphere-assembled substrate, (ii) formation of ZnO seeds on PS microspheres, and (iii) growth of ZnO into spiky nanostructures.

2.2.1. Preparation of the PS Microsphere-Assembled Substrate. PS microspheres were assembled on the glass substrate using a Langmuir−Blodgett (LB) instrument (KSV-NIMA-LB) (Figure S1). The dispersion of the negatively charged PS microspheres in a mixture of water and ethanol (5 mg mL^{-1}) was spread on a water surface and compressed with a barrier moving at a speed of 2 mm min^{-1}. When the surface pressure reached 45 mN m^{-1}, the glass slide was lifted to obtain a monolayer of closely packed PS microspheres on the glass slide. The glass slide deposited with PS microspheres was thermally treated at 100 °C for 10 min to facilitate the adhesion of PS microspheres to the glass slide.

2.2.2. Formation of ZnO Nanoparticles on PS Microspheres. ZnO seeds were formed by adding a solution of $Zn(CH_3COO)_2$ and KOH dropwise to methanol at 60 °C, followed by continuous stirring for 2 h. The glass slide with a layer of PS was immersed in the ZnO seed solution for 10 min and then dried at room temperature. This process was repeated three times to form ZnO nanocrystal layers onto PS by electrostatic adsorption between the negatively charged PS surface and positively charged ZnO nanocrystals.

2.2.3. Growth of ZnO Hedgehog Structure Films. ZnO nanoparticle layers were immersed in a ZnO growth precursor solution consisting of zinc nitrate hexahydrate ($Zn(NO_3)_2 \cdot 6H_2O$) and hexamethylenetetramine (HMTA). ZnO spikes were grown at 90 °C for 6 h using a hydrothermal process. The ZnO hedgehog structures were then immersed in ethanol, sonicated for 10 s, rinsed again in ethanol, and dried in an oven.

2.3. Synthesis of Graphene Quantum Dots (GQDs). The GQDs were prepared by chemical oxidation of biomass-derived graphene (BG) (Figure S2). The synthesis method of BG is described in detail in our previous study.[24] For the synthesis of GQDs, 100 mg of BG was added to 65 mL of 6 M HNO_3 and refluxed at 120 °C for 24 h. After the mixture was cooled to room temperature, the product was centrifuged to separate the GQDs. The brown supernatant was then neutralized with KOH and concentrated using a rotary evaporator at 100 °C. Subsequently, the GQDs were purified using a dialysis bag (MWCO 2000 Da) for 3 days, with the washing water changed every 12 h. Finally, the aqueous suspension of GQDs was stored in a refrigerator at 5 °C for further experiments.

2.4. Preparation of Hedgehog ZnO and GQD Heterojunction Photocatalysts. The assembly of GQDs on the ZnO substrate was performed as follows: the ZnO substrate was immersed in a polyethylenimine (PEI) (1.0 mg mL^{-1})-added NaCl solution (pH = 7) for 10 min and dried under vacuum for 30 min (Scheme 1c). Subsequently, the substrate was immersed in the aqueous suspension of GQDs for 10 min and dried under vacuum for 30 min. This dipping process was repeated twice to fabricate the ZnO/GQD substrate.

2.5. Photocatalytic Water Splitting. The photocatalytic water-splitting reaction was carried out in a Pyrex round-bottom flask (Figure S3). The sample substrate was placed in a 250 mL two-neck round-bottom flask containing 200 mL of DI water. The substrate was fixed in place by a pole leaning on the flask neck. A 300 W xenon lamp with a UV cut filter was used for visible light irradiation. During light illumination, the heat generated was controlled by a glass water bath. Collected gases were obtained in an inverted measuring tube placed in another water bath containing diluted HCl. The concentration of the evolved hydrogen was analyzed by gas chromatography at various intervals. The apparent quantum yield (AQY) was calculated using the equation provided in the Supporting Information.

2.6. Electrochemical Measurement. Electrochemical analysis was carried out using a platinum plate as the counter electrode and an Ag/AgCl electrode as the reference electrode. An aqueous solution of Na_2SO_4 (0.5 M) was used as the electrolyte without any additives. The working electrode was prepared on indium tin oxide (ITO) as the sample substrate. The area of the working electrode was 3.0 cm^2 (1 × 3 cm). The experiment was conducted under darkroom light control by ON and OFF states of a 300 W xenon light, using a 420 nm optical filter for visible light measurement.

2.7. Characterizations. Scanning electron microscopy (SEM), transmission electron microscopy (TEM), and high-resolution transmission electron microscopy (HR-TEM) were used to examine the morphology of ZnO, GQDs, and the ZnO/GQDs composite. The elemental compositions of ZnO/GQDs were analyzed by X-ray photoelectron spectroscopy (XPS) with a monochromatic Al Kα source. Fourier transform infrared (FTIR) spectroscopy was used to identify functional groups present in ZnO/GQDs over the range of 400−4000 cm^{-1}. Hydrogen gas was measured by a gas chromatography (Agilent 8890 GC) system with a thermal conductivity detector (TCD) and argon as the gas carrier using an HP-5 column with 30 m length, 320 μm diameter, and 0.25 μm film thickness under specific conditions.

3. RESULTS AND DISCUSSION

3.1. Characterization of Hedgehog ZnO Nanostructures and Graphene Quantum Dots (GQDs). Scanning electron microscopy (SEM) was utilized to characterize the hedgehog-shaped ZnO nanostructures and the ZnO/GQDs heterostructure. The hedgehog ZnO nanostructures were synthesized on a polystyrene (PS) microsphere assembled on a glass substrate by using the Langmuir−Blodgett (LB) technique, as illustrated in Figure 1a.

SEM imaging revealed the distinct spiky morphology of the ZnO nanostructures, featuring an average spike length of approximately 800 nm and a diameter of 45 nm with a dense arrangement of spikes per unit area (Figures 1b and S4). Initially, ZnO exhibited a hedgehog-like morphology with well-defined, rod-like projections radiating from a central core. Subsequently, GQDs were deposited on the surface of spiky ZnO nanostructures, which had been functionalized with polyethylenimine (PEI). This PEI functionalization enhanced the interaction between ZnO and GQDs, promoting their integration and facilitating interfacial charge transfer processes. The ZnO/GQDs heterostructures displayed noticeable changes in surface texture compared with the pristine ZnO nanostructures, indicating the successful incorporation of GQDs onto the ZnO nanostructure (Figure 1c). Elemental mapping further confirmed the successful deposition of GQDs on the ZnO nanostructure (Figure S5).

https://doi.org/10.1021/acsomega.4c05574
ACS Omega 2024, 9, 40790−40800

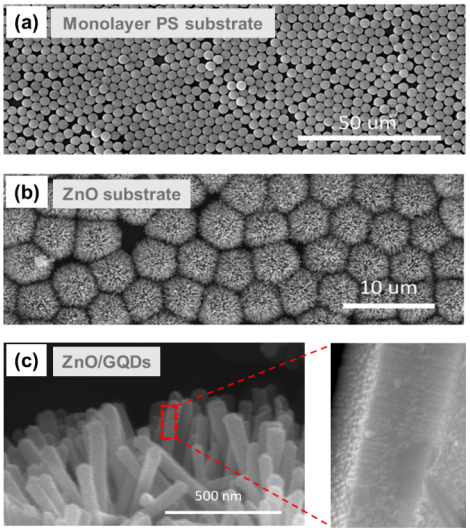

Figure 1. SEM images: (a) monolayer of PS microspheres on a glass slide, (b) hedgehog-shaped ZnO formed on PS microspheres, and (c) the ZnO/GQDs heterostructure.

GQDs for this study were synthesized through strong acid treatment with biomass-derived graphene as the precursor. The synthesized GQDs were characterized to elucidate their structural and optical properties. Transmission electron microscopy (TEM) imaging revealed a uniform size distribution of the GQDs, with an average diameter of approximately 5 nm (Figure 2a).

UV−visible spectroscopy confirmed the presence of characteristic absorption peaks in the visible range. A strong absorption between 250 and 300 nm corresponds to the $\pi-\pi^*$ transition in the sp^2-bonded carbon network of graphene-based materials. An absorption shoulder at approximately 380 nm corresponds to the electron transition from the *n*-orbital induced by the electron-donating —C═O group on GQDs to the π^* orbital. An absorption tail extending up to 600 nm results from the *n*-orbital induced by the electron-donating N on GQDs to the π^* orbital (Figure 2b).[25−28]

These observations confirm the presence of aromatic conjugated structures and oxygen- and nitrogen-containing functional groups in the GQDs, which play crucial roles in their photoluminescence (PL) properties. PL spectroscopy was performed to further examine the emission behavior of the GQDs under different excitation wavelengths ranging from 360 to 620 nm (Figure 2c). The observed excitation-dependent PL behavior, with a shift in the emission wavelength as the excitation wavelength changes, is a characteristic signature of the quantum confinement effect. Due to the quantum confinement effect and small size, nanoscale GQDs behave like semiconductor materials.[28−30] Additionally, the GQDs were prepared by chemical oxidation of graphene-based materials to have defects and oxygen functional groups, which is attributed to the generation of discrete energy levels and photoluminescence properties. When excited with wavelengths ranging from 360 to 440 nm, the PL spectra exhibited an excitation-dependent feature and slight down-conversion, indicating the discrete energy levels of the confined charge carriers rather than the continuous energy bands of bulk graphene. As the excitation wavelength increased from 460 to 620 nm, the emission peak gradually red-shifted from 550 to 650 nm, with the strongest emission peak observed at 580 nm for an excitation wavelength of 520 nm. This excitation-dependent behavior and the observed Stokes shift arise from the difference in the energy levels involved in the absorption and emission processes, indicating the presence of the quantum confinement effect and different surface states with oxygen-containing groups in the GQDs.[27] Additionally, the rapid decrease in intensity with an increasing excitation wavelength suggests the presence of emissive free sites within the GQD structure, further supporting the presence of the quantum confinement phenomenon. The inset of Figure 2c showcases the bright yellow-orange PL of the GQDs under a 365 nm UV lamp, further highlighting the effects of the quantum confinement and surface functional groups.[28]

Figure 3 depicts the Fourier transform infrared (FTIR) spectrum of hedgehog ZnO and ZnO/GQDs heterostructures,

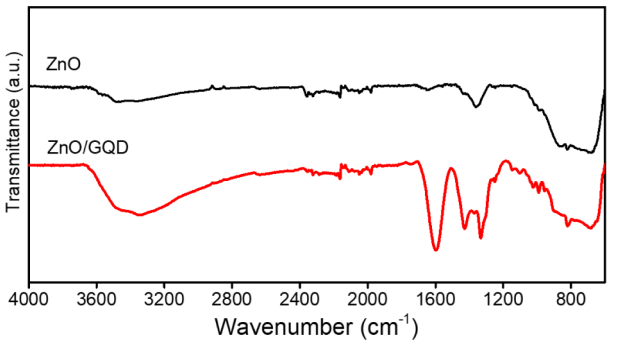

Figure 3. FTIR spectra of ZnO/GQDs, showing the characteristic vibrational modes and functional groups present in the heterostructure.

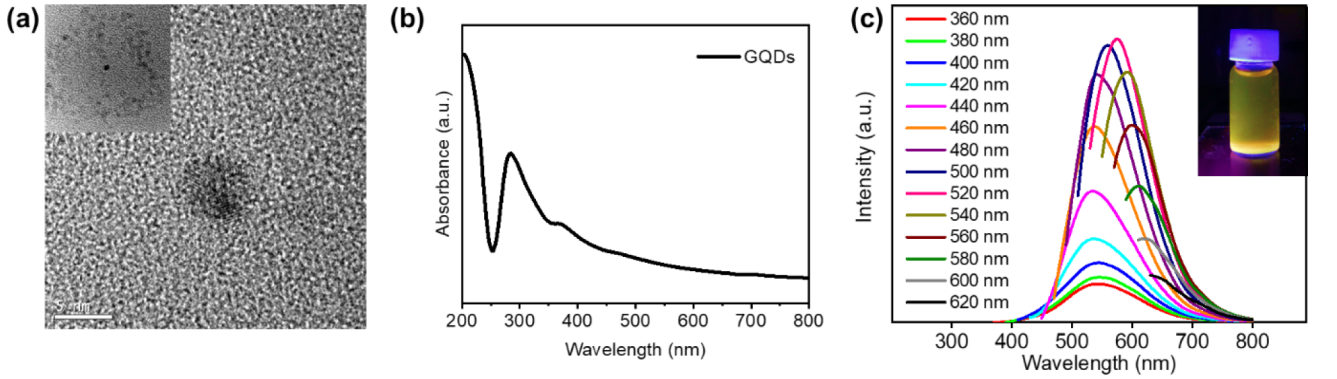

Figure 2. (a) TEM images of GQDs, showing their size and morphology. (b) UV−visible absorption spectrum of GQDs, showing characteristic absorption peaks. (c) PL spectra of GQDs, illustrating excitation-dependent emission behavior.

https://doi.org/10.1021/acsomega.4c05574
ACS Omega 2024, 9, 40790−40800

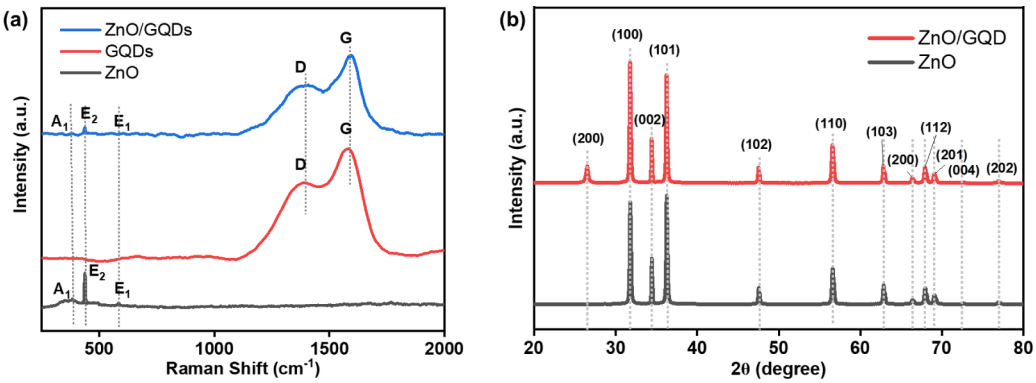

Figure 4. (a) Raman spectra of ZnO, GQDs, and the ZnO/GQDs heterostructure. (b) XRD patterns of ZnO and the ZnO/GQDs heterostructure.

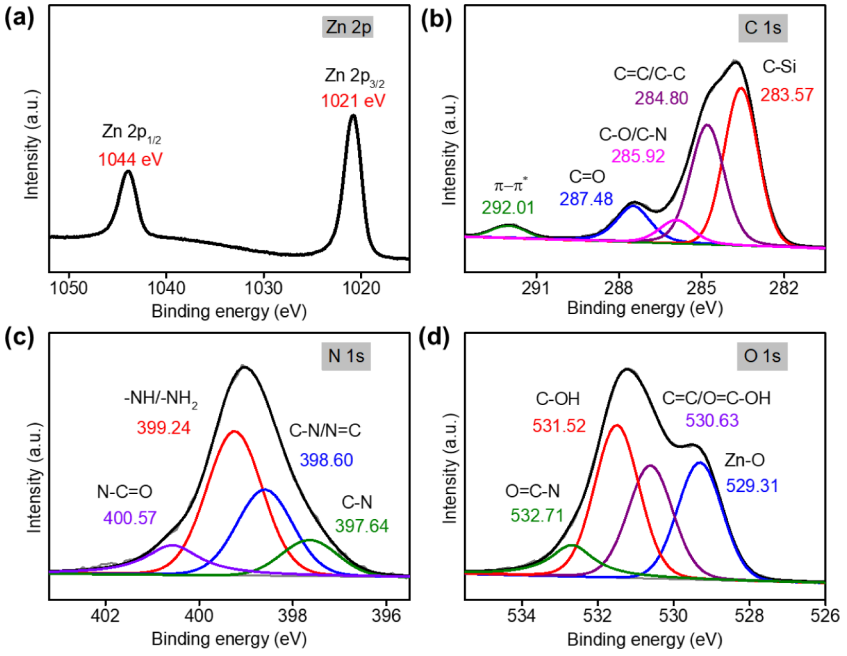

Figure 5. XPS analysis of the ZnO/GQDs heterostructure: (a) Zn 2p, (b) C 1s, (c) N 1s, and (d) O 1s spectra.

elucidating the chemical functional groups within the heterostructure. The broad signal between 3000 and 3700 cm^{-1} corresponds to the stretching vibrations of −NH and −OH groups, confirming the presence of amine and carboxyl functional groups within the ZnO/GQDs heterostructure.[31−33] Additionally, a strong absorption band at 1597 cm^{-1} is attributed to the amide group —(C═O)NH— of PEI.[32] Furthermore, distinct peaks corresponding to vibrations of the amine group and C−N single bond stretching were observed at 1330 and 1104 cm^{-1}, further confirming the presence of functional groups on the surface of GQDs.[34] Finally, the absorption peak at 678 cm^{-1} corresponds to the Zn−O stretching vibration, indicating the bonding of GQDs to the surface of the ZnO nanostructure.[35] These FTIR spectra findings corroborate the SEM observations, providing further evidence that GQDs are indeed bonded to the surface of ZnO within the heterostructure.

The Raman spectra further confirm the formation of the ZnO/GQDs heterostructures (Figure 4a).

The ZnO/GQDs heterostructure exhibits characteristic peaks associated with GQDs, specifically the D-band at 1387 cm^{-1} and the G-band at 1580 cm^{-1}.[19,24] The intensity ratio of the D-band to the G-band (I_D/I_G = 0.89) is higher in the heterostructure compared to the GQDs alone (I_D/I_G = 0.81), indicating a reduction in the size of the sp^2-hybridized carbon domains of GQDs due to the interaction with ZnO.[21] Additionally, the ZnO peak at 437 cm^{-1}, associated with the high-frequency E_2 mode, is slightly shifted in the heterostructure, suggesting a modification of the ZnO structure due to interaction with GQDs. The peaks at 583 and 384 cm^{-1} in both ZnO and the ZnO/GQDs heterostructure indicate structural defects within ZnO.[19,21] The X-ray diffraction (XRD) patterns (Figure 4b) show characteristic peaks for ZnO at 2θ values of 31.77°, 34.42°, and 36.25°, among others, corresponding to the various crystal planes of the wurtzite ZnO structure.[36,37] In the ZnO/GQDs heterostructure, the ZnO peaks remain present but with some variations in peak intensities compared to the ZnO nanostructure. Additional peaks at 2θ values of 26.50° and 54.55°, corresponding to the (002) and (004) planes of GQDs, confirm the presence of GQDs within the heterostructure.[19] The increased intensity of the (101) peak in the ZnO/GQDs suggests a higher level of defect, likely due to lattice disorder and strain within the ZnO structure induced by the inclusion of GQDs.[19,21]

X-ray photoelectron spectroscopy (XPS) analysis was conducted to investigate the chemical composition, surface

https://doi.org/10.1021/acsomega.4c05574
ACS Omega 2024, 9, 40790−40800

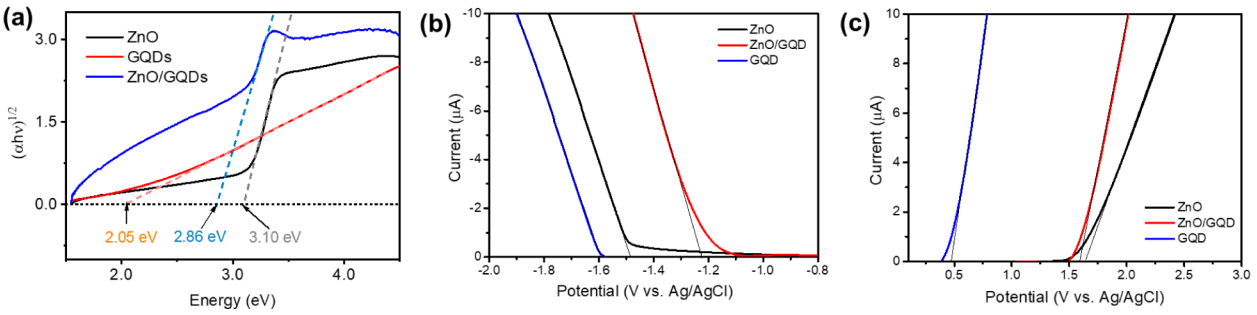

Figure 6. (a) Optical band gap measurements using Tauc's plot for ZnO, GQDs, and the ZnO/GQDs heterostructure. (b) Cathodic linear sweep voltammetry and (c) anodic linear sweep voltammetry of ZnO, GQDs, and the ZnO/GQDs heterostructure.

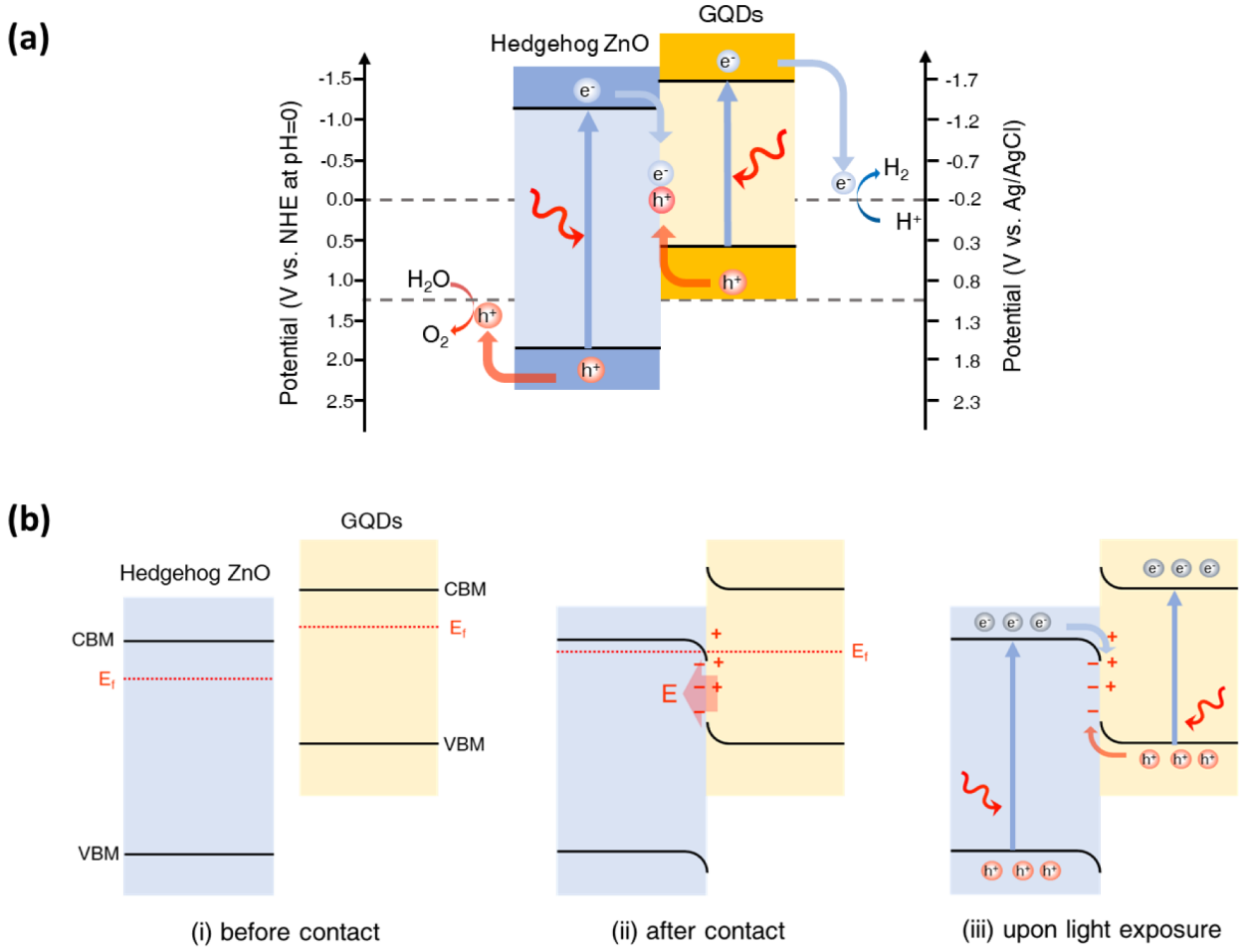

Figure 7. (a) Schematic illustration of the energy level diagram and photocatalytic water splitting of the ZnO/GQDs heterostructure. (b) Charge carrier transfer process in S-scheme mode.

chemical states, and bonding configuration of the ZnO/GQDs heterostructures. The survey spectrum (Figure S6a,b) revealed the presence of core elements including Zn, C, O, and N in the ZnO and ZnO/GQDs heterostructure. The significant increase in the C 1s peak intensity observed in the ZnO/GQDs compared to ZnO suggests that a substantial amount of GQDs was successfully deposited on the surface of the ZnO structure. The high-resolution XPS spectra of the core elemental peaks for the ZnO/GQDs heterostructure and ZnO are presented in Figures 5 and S6c,d, respectively. The Zn 2p spectrum of both ZnO and ZnO/GQDs heterostructure (Figure 5a) exhibited two distinct peaks at 1044 and 1021 eV, corresponding to Zn $2p_{1/2}$ and Zn $2p_{3/2}$, respectively.[38] This suggests the presence of Zn^{2+} in the oxidation state and indicates that the deposition of GQDs did not alter the chemical state of ZnO.[39] The C 1s XPS spectrum was deconvoluted into five peaks (Figure 5b). The peak at 283.57 eV corresponds to the C−Si bond originating from GQDs on the glass substrate. The peak at 284.8 eV is attributed to sp^2-hybridized carbon (C═C/C−C) in the aromatic rings of GQDs.[40,41]

Analysis of the N 1s peak (Figure 5c) revealed four peaks. The peak at 399.24 eV indicated the presence of amine groups (−NH or $-NH_2$). The peak at 398.60 eV was attributed to the existence of pyridinic N (C═N—C) in its sp^2-hybridized form. The O═C—N group, resulting from the PEI bonding between ZnO and GQDs, appeared in both N 1s and O 1s deconvoluted spectra

https://doi.org/10.1021/acsomega.4c05574
ACS Omega 2024, 9, 40790−40800

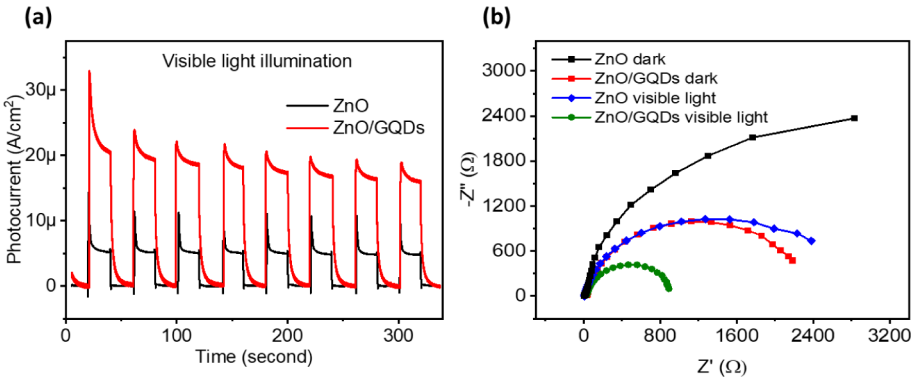

Figure 8. (a) Transient photocurrent response comparison between ZnO and the ZnO/GQDs heterostructure. (b) Nyquist plot showing the charge transfer resistance for ZnO and ZnO/GQDs.

(Figure 5d) at 532.71 and 400.57 eV, respectively.[42] The peak observed at a binding energy of 529.31 eV was assigned to the O^{2-} ions, representing oxygen in the oxide lattice without oxygen vacancies, indicating Zn−O bonding. This peak was present in both ZnO and the ZnO/GQDs composite, suggesting that the integration of GQDs onto the ZnO surface preserves the ZnO lattice structure.[43]

UV−vis spectroscopy was employed to determine the optical bandgaps of ZnO, GQDs, and the ZnO/GQDs heterostructure. The band gaps were determined using the Tauc plot method (Figure 6a), revealing values of 3.10 eV for ZnO, 2.05 eV for GQDs, and 2.86 eV for the ZnO/GQDs.

Linear sweep voltammetry (LSV) analysis was conducted to further determine the conduction band minimum (CBM), valence band maximum (VBM), and the bandgaps of the materials.[22] According to the LSV data (Figure 6b,c), the CBMs of the ZnO, GQDs, and ZnO/GQDs were found to be −1.47, −1.60, and −1.21 V (vs Ag/AgCl), respectively. The corresponding VBMs were 1.63, 0.48, and 1.59 V (vs Ag/AgCl), respectively. The bandgap values determined by the LSV method are consistent with those derived from the Tauc plot, validating the measurements. The reduced band gap energy of the ZnO/GQDs heterostructure suggests enhanced light absorption capabilities, particularly within the visible range, compared to the ZnO nanostructure. This reduced band gap implies that the ZnO/GQDs heterostructure can generate a greater number of photoexcited carriers under solar irradiation, thereby augmenting its photocatalytic activity.[21,44]

Considering that the CBM of GQDs is positioned higher than that of ZnO, while the VBM of ZnO is lower than that of GQDs, we propose an S-scheme heterojunction mechanism for ZnO/GQDs photocatalysis. The energy band diagram (Figure 7a) illustrates the key transitions involved in water splitting.

In this mechanism, the alignment of the CBM and VBM upon contact drives effective charge separation, establishing a staggered energy band structure conducive to efficient photocatalysis. Upon contact, the Fermi energy levels of ZnO and GQDs align, resulting in band bending that distorts the original band diagrams. The band edge of GQDs bends upward as a result of the loss of electrons, whereas the band edge of ZnO bends downward due to the accumulation of electrons, as illustrated in Figure 7b.[45] This bending creates an internal electric field due to electrons spontaneously migrating from GQDs to ZnO, which drives the separation of the photogenerated charge carriers. Electrons in the CB of ZnO and holes in the VB of GQDs are driven directly toward the interface of ZnO and GQDs. This internal field reduces the possibility of electron−hole recombination due to the Schottky barrier at the ZnO/GQDs interface, effectively extending the lifetime of the charge carriers. Consequently, electrons in the CB of GQDs facilitate the reduction reaction to produce hydrogen, while holes in the VB of ZnO drive the oxidation reaction to generate oxygen. Furthermore, the S-scheme heterojunction allows weak reduction electrons in the CBM of ZnO to recombine with the weak oxidation holes in the VBM of GQDs, accelerating charge carrier separation while maintaining a strong redox potential. This synergistic effect, driven by the S-scheme heterojunction, significantly enhances the photocatalytic efficiency of the ZnO/GQDs heterostructure for water splitting.[21,46,47]

The transient photocurrent response of ZnO and ZnO/GQDs under visible light irradiation (λ > 420 nm) was investigated using an electrochemical workstation with a 300 W xenon lamp and UV-cut filter (Figure 8). As depicted in Figure 8a, ZnO particles exhibited a weaker photocurrent response, whereas the ZnO/GQDs heterostructure displayed a significantly stronger photocurrent response, approximately three times higher than that of ZnO alone. The subdued photocurrent response observed for ZnO under visible light is attributed to its relatively large bandgap energy (3.10 eV), which limits its absorption of visible light. Conversely, the augmented photocurrent in ZnO/GQDs suggests a higher charge transfer rate due to improved light absorption, efficient charge separation, and reduced recombination of electron−hole pairs. It is worth noting that the photocurrent for both ZnO and ZnO/GQDs slightly weakened with prolonged light exposure, likely due to photocorrosion.[19,48]

To further elucidate the charge separation efficiency of the ZnO/GQDs heterostructure under visible light irradiation, electrochemical impedance spectroscopy (EIS) measurements were conducted (Figure 8b). The Nyquist plots reveal that the semicircle diameter, representing internal resistance, is smaller for ZnO and ZnO/GQDs under visible light irradiation than that under dark conditions. This reduction in the radius indicates a lower charge transfer resistance, signifying efficient charge transfer at the electrode−electrolyte interface.[49,50] The smaller semicircle for ZnO/GQDs compared to ZnO in the dark suggests that the addition of GQDs reduces the charge transfer resistance at the electrode−electrolyte interface for the ZnO/GQDs system. GQDs can act as electron acceptors and facilitate the separation of electron−hole pairs generated in ZnO, thereby preventing recombination. The reduced resistance in both ZnO and ZnO/GQDs under light illumination underscores rapid

https://doi.org/10.1021/acsomega.4c05574
ACS Omega 2024, 9, 40790−40800

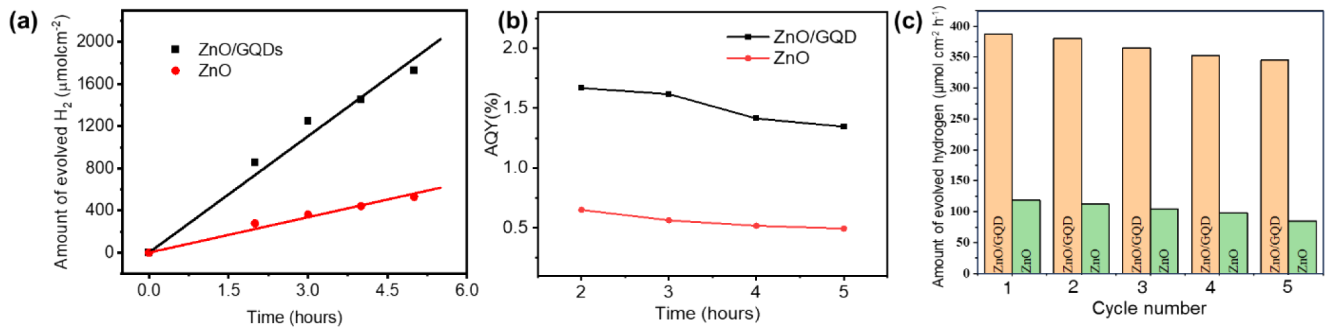

Figure 9. (a) Hydrogen evolution performance over time for ZnO and ZnO/GQDs. (b) Apparent quantum yield (AQY) for ZnO and ZnO/GQDs during photocatalytic water splitting. (c) Hydrogen evolution over repeated cycles for ZnO and ZnO/GQDs.

charge transfer and increased photocurrent generation, corroborating the transient photocurrent results. GQDs can also act as light-harvesting centers, absorbing visible light and generating electron−hole pairs, which can provide efficient pathways for charge transport, leading to reduced charge transfer resistance. Therefore, the significant enhancement in photocurrent response and reduced charge transfer resistance under visible light confirm the superior photocatalytic activity of the ZnO/GQDs heterostructure. This improvement can be attributed to the synergistic effects of the GQDs, which not only narrow the bandgap but also facilitate efficient charge separation and transfer, thereby enhancing photocatalytic performance for water splitting.

The photocatalytic performance for hydrogen production was evaluated using gas chromatography (GC) equipment coupled with a xenon lamp and UV-cut filters (Figure 9).

As shown in Figure 9a, hydrogen (H_2) evolution increased almost linearly with the light irradiation time. Notably, the level of H_2 production from the ZnO/GQDs heterostructure was significantly higher than that from pristine ZnO, consistent with the photocurrent response data. The average H_2 evolution rates were 387.90 μmol cm^{-2} h^{-1} for the ZnO/GQDs heterostructure and 118.98 μmol cm^{-2} h^{-1} for the pristine ZnO hedgehog structure. This more than 3-fold increase in H_2 production from the ZnO/GQDs heterostructure compared to pristine ZnO suggests more efficient charge separation and reduced charge recombination in the ZnO/GQDs heterostructure. Figure 9b presents the apparent quantum yield (AQY) for hydrogen production at 440 nm, which was 1.51% for the ZnO/GQDs heterostructure and 0.56% for pristine ZnO, averaged over 5 h of reaction. The ZnO/GQDs heterostructure maintained its photocatalytic activity stably over prolonged reactions, demonstrating remarkable stability as a photocatalyst. Reusability tests for hydrogen production under light (using a 420 nm filter) are shown in Figure 9c. The ZnO/GQDs heterostructure maintained good stability up to the fifth cycle with only an 11% reduction in the degradation rate by the fifth cycle.

A comparison of the present study with previous reports on different photocatalysts used in water splitting is provided in Table 1. This comparison highlights the superior performance of the ZnO/GQDs heterostructure in terms of hydrogen production efficiency and stability, underscoring its potential as an effective photocatalyst for sustainable hydrogen generation.

Table 1. Comparison of Hydrogen Production Performance and Apparent Quantum Yield (AQY, %) Under Light Illumination for Various Photocatalysts

Material	H_2 production (μmol h^{-1}/unit)	Light source	AQY (%)	ref.
ZnO	22.32 (gram)	solar light		51
ZnO	256 (gram)	visible light		52
ZnO	42 (gram)	solar light	1.02	53
ZnO	8.7 (gram)	UV−visible light		54
ZnO	118.98 (cm^2)	visible light	0.56 (440 nm)	this study
ZnO/Lu	1380 (gram)	visible light		52
ZnO/CdS	334.8 (gram)	solar light		51
ZnO/CdS	4134 (gram)	UV−visible light		55
ZnO/Au/CdS	502.20 (gram)	solar light		51
ZnO/g-C_3N_4	827.5 (gram)	solar light	20.00	53
ZnO/g-C_3N_4	123 (gram)	UV−visible light	1.13 (240 nm)	54
ZnO/In_2O_3	240.4 (gram)	visible light		56
TiO_2/S,N-GQDs	86 (gram)	visible light		57
GQDs/PDI	1600 (gram)	visible light	0.50 (420 nm)	58
CQDs/CdS	3928 (gram)	visible light	2.20 (400 nm)	59
N-CQDs/CdS	907 (gram)	visible light	20.98 (400 nm)	59
N-GQDs/PTI/ZnO-QDs	880 (gram)	visible light		60
N,p-CQDs/ZnO	417 (gram)	visible light		36
ZnO/CDs	250 (cm^2)	solar light		61
ZnO/GQDs	387.91 (cm^2)	visible light	1.51 (440 nm)	this study

4. CONCLUSIONS

In conclusion, we successfully developed a novel heterostructure comprising hedgehog-shaped zinc oxide (ZnO) nanostructures coupled with graphene quantum dots (GQDs) to enhance photocatalytic water splitting. The integration of GQDs with ZnO nanostructures resulted in a significant enhancement of photocatalytic activity by extending light absorption into the visible spectrum, facilitating efficient charge separation and reducing charge recombination. Characterization studies confirmed the successful synthesis of well-defined ZnO nanostructures and GQDs, with transmission electron microscopy (TEM) showing a uniform size distribution of GQDs of approximately 5 nm in diameter. UV−visible spectroscopy and photoluminescence (PL) spectroscopy revealed the optical properties of GQDs, including visible range absorption and

https://doi.org/10.1021/acsomega.4c05574
ACS Omega 2024, 9, 40790−40800

excitation-dependent emission behavior, indicative of quantum confinement effects and surface functional groups on GQDs. The ZnO/GQDs heterostructure exhibited a reduced band gap energy compared to ZnO alone, resulting in enhanced light absorption and a significantly higher photocurrent response under visible light irradiation. Electrochemical impedance spectroscopy (EIS) measurements further confirmed efficient charge transfer at the ZnO/GQDs interface, highlighting active charge transfer and increased photocurrent generation. Photocatalytic evaluation revealed that the ZnO/GQDs heterostructure achieved over 3-fold higher hydrogen (H_2) production rates compared to pristine ZnO, along with a superior apparent quantum yield (AQY) for hydrogen production. Importantly, the ZnO/GQDs heterostructure maintained stable photocatalytic activity over prolonged reactions, underscoring its good stability as a photocatalyst. This study demonstrates the promising potential of the ZnO/GQDs heterostructure as an efficient photocatalyst for sustainable hydrogen generation through water splitting. The synergistic effects between ZnO nanostructures and GQDs provide insights for the design and development of next-generation photocatalysts for renewable energy applications. Further research into optimizing the heterostructure configuration and exploring additional functionalities of GQDs could lead to even more efficient photocatalytic systems for practical implementation in solar energy conversion technologies.

■ ASSOCIATED CONTENT

Supporting Information

The Supporting Information is available free of charge at https://pubs.acs.org/doi/10.1021/acsomega.4c05574.

Band-gap energy calculations; apparent quantum yield calculations; illustration of the Langmuir−Blodgett (LB) deposition method, GQD synthesis, and water-splitting experimental setup; XPS survey spectra (PDF)

■ AUTHOR INFORMATION

Corresponding Author

TaeYoung Kim − *Department of Science Materials and Engineering, Gachon University, Seongnam-si, Gyeonggi-do 13120, Republic of Korea;* orcid.org/0000-0001-8156-4438; Email: taeykim@gachon.ac.kr

Authors

Thi Kieu Oanh Le − *Department of Science Materials and Engineering, Gachon University, Seongnam-si, Gyeonggi-do 13120, Republic of Korea; School of Environment and Science, Griffith University, Southport, Queensland 4215, Australia*

Mitesh Ganpat Mapari − *Department of Science Materials and Engineering, Gachon University, Seongnam-si, Gyeonggi-do 13120, Republic of Korea*

Complete contact information is available at: https://pubs.acs.org/10.1021/acsomega.4c05574

Author Contributions

#T.K.O.L and M.G.M contributed equally. The manuscript was written through the contributions of all authors. All authors have given approval to the final version of the manuscript.

Notes

The authors declare no competing financial interest.

■ ACKNOWLEDGMENTS

This work was supported by the National Research Foundation of Korea (NRF) grant funded by the Korea government (MSIT) (No. 2022R1A2C1093082). This work was supported by the Gachon University research fund of 2019 (GCU-2019-0832). This work was supported by the Gachon University research fund of 2021 (GCU-202106550001).

■ REFERENCES

(1) Wang, M.; et al. Review of renewable energy-based hydrogen production processes for sustainable energy innovation. *Global Energy Interconnect.* **2019**, *2* (5), 436−443.

(2) Christopher, K.; Dimitrios, R. A review on exergy comparison of hydrogen production methods from renewable energy sources. *Energy Environ. Sci.* **2012**, *5* (5), 6640−6651.

(3) Gielen, D.; Taibi, E.; Miranda, R. *Hydrogen: a renewable energy perspective*; International Renewable Energy Agency: Abu Dhabi, 2019.

(4) Ta, Q. T. H.; Tran, N. M.; Noh, J.-S. Rice Crust-Like ZnO/Ti3C2Tx MXene Hybrid Structures for Improved Photocatalytic Activity. *Catalysts* **2020**, *10* (10), 1140.

(5) Zhu, D.; Zhou, Q. Action and mechanism of semiconductor photocatalysis on degradation of organic pollutants in water treatment: A review. *Environ. Nanotechnol., Monit. Manage.* **2019**, *12*, 100255.

(6) Ta, Q. T. H.; Namgung, G.; Noh, J.-S. Facile synthesis of porous metal-doped ZnO/g-C3N4 composites for highly efficient photocatalysts. *J. Photochem. Photobiol., A* **2019**, *368*, 110−119.

(7) Zhong, S.; et al. Hybrid cocatalysts in semiconductor-based photocatalysis and photoelectrocatalysis. *J. Mater. Chem. A* **2020**, *8* (30), 14863−14894.

(8) Ta, Q. T. H.; Tran, N. M.; Tri, N. N.; Sreedhar, A.; Noh, J.-S.; et al. Highly surface-active Si-doped TiO2/Ti3C2Tx heterostructure for gas sensing and photodegradation of toxic matters. *Chem. Eng. J.* **2021**, *425*, 131437.

(9) Nadeem, M. A.; et al. An overview of the photocatalytic water splitting over suspended particles. *Catalysts* **2021**, *11* (1), 60.

(10) Jo, W. J.; et al. Phase transition-induced band edge engineering of BiVO4 to split pure water under visible light. *Proc. Natl. Acad. Sci. U. S. A.* **2015**, *112* (45), 13774−13778.

(11) Moniz, S. J. A.; et al. Visible-light driven heterojunction photocatalysts for water splitting − a critical review. *Energy Environ. Sci.* **2015**, *8* (3), 731−759.

(12) Zhang, X.; Peng, T.; Song, S. Recent advances in dye-sensitized semiconductor systems for photocatalytic hydrogen production. *J. Mater. Chem. A* **2016**, *4* (7), 2365−2402.

(13) Kumaravel, V.; et al. Photocatalytic hydrogen production using metal doped TiO2: A review of recent advances. *Appl. Catal., B* **2019**, *244*, 1021−1064.

(14) Martha, S.; Sahoo, P. C.; Parida, K. M. An overview on visible light responsive metal oxide based photocatalysts for hydrogen energy production. *RSC Adv.* **2015**, *5* (76), 61535−61553.

(15) Wang, G.; Chang, J.; Tang, W.; Xie, W.; Ang, Y. S.; et al. 2D materials and heterostructures for photocatalytic water-splitting: a theoretical perspective. *J. Phys. D: appl. Phys.* **2022**, *55* (29), 293002.

(16) Shanker, G. S.; Biswas, A.; Ogale, S. 2D materials and their heterostructures for photocatalytic water splitting and conversion of CO2 to value chemicals and fuels. *J. Phys. Energy* **2021**, *3* (2), 022003.

(17) Zhang, H.; Gao, Y.; Meng, S.; Wang, Z.; Wang, P.; Wang, Z.; Qiu, C.; Chen, S.; Weng, B.; Zheng, Y.-M. Metal Sulfide S-Scheme Homojunction for Photocatalytic Selective Phenylcarbinol Oxidation. *Adv. Sci.* **2024**, *11* (17), No. e2400099.

(18) Meng, S.; Chen, C.; Gu, X.; Wu, H.; Meng, Q.; Zhang, J.; Chen, S.; Fu, X.; Liu, D.; Lei, W. Efficient photocatalytic H2 evolution, CO2 reduction and N2 fixation coupled with organic synthesis by cocatalyst and vacancies engineering. *Appl. Catal., B* **2021**, *285*, 119789.

(19) Kumar, S.; et al. ZnO-graphene quantum dots heterojunctions for natural sunlight-driven photocatalytic environmental remediation. *Appl. Surf. Sci.* **2018**, *447*, 802−815.

(20) Ebrahimi, M.; et al. Improved Solar-Driven Photocatalytic Activity of Hybrid Graphene Quantum Dots/ZnO Nanowires: A Direct Z-Scheme Mechanism. *ACS Sustainable Chem. Eng.* **2017**, *5* (1), 367−375.
(21) Ning, X., et al. *Constructing of GQDs/ZnO S-scheme heterojunction as efficient piezocatalyst for environmental remediation and understanding the charge transfer mechanism*, Elsevier: Carbon, 2024; Vol. *218*; pp. 118772.
(22) Yan, Y.; et al. Systematic Bandgap Engineering of Graphene Quantum Dots and Applications for Photocatalytic Water Splitting and CO(2) Reduction. *ACS Nano* **2018**, *12* (4), 3523−3532.
(23) Xie, B. W.; et al. Radiative properties of hedgehog-like ZnO-Au composite particles with applications to photocatalysis. *J. Quant. Spectrosc. Radiat. Transfer* **2018**, *217*, 1−12.
(24) Le, T. K. O.; Jung, S.; Pham, T. H.; Kim, T.; et al. Highly porous biomass-derived graphene-based carbons for removal of phenol from wastewater. Colloids and Surfaces A. *Colloids Surf., A* **2024**, *699*, 134588.
(25) Zhang, M.; Bai, L.; Shang, W.; Xie, W.; Ma, H.; Fu, Y.; Fang, D.; Sun, H.; Fan, L.; Han, M; et al. Facile synthesis of water-soluble, highly fluorescent graphene quantum dots as a robust biological label for stem cells. *J. Mater. Chem.* **2012**, *22* (15), 7461.
(26) Zhang, P.; et al. Electrospinning graphene quantum dots into a nanofibrous membrane for dual-purpose fluorescent and electrochemical biosensors. *J. Mater. Chem. B* **2015**, *3* (12), 2487−2496.
(27) Perini, G.; Palmieri, V.; Ciasca, G.; De Spirito, M.; Papi, M.; et al. Unravelling the Potential of Graphene Quantum Dots in Biomedicine and Neuroscience. *Int. J. Mol. Sci.* **2020**, *21* (10), 3712.
(28) Yeh, T. F.; et al. Elucidating Quantum Confinement in Graphene Oxide Dots Based On Excitation-Wavelength-Independent Photoluminescence. *J. Phys. Chem. Lett.* **2016**, *7* (11), 2087−2092.
(29) Khan, M. J.; Wibowo, A.; Sakdaronnarong, C. Two-Dimensional Graphene Quantum Dots in Drug Delivery Applications. In *Two-dimensional Hybrid Composites: synthesis, Properties and Applications*; Springer, 2024; pp. 279294.
(30) Liu, Y. *Photoluminescence Mechanism and Applications of Graphene Quantum Dots*, University of Kentucky; 2017.
(31) Das, S. C.; Majumdar, A.; Shripathi, T.; Hippler, R.; et al. Note: Development of fast heating inert gas annealing apparatus operated at atmospheric pressure. *Rev. Sci. Instrum.* **2012**, *83* (4), 046109.
(32) Majumdar, A.; et al. Role of nitrogen in the formation of HC− N films by CH4/N2 barrier discharge plasma: Aliphatic tendency. *J. Phys. Chem. B* **2009**, *113* (48), 15734−15741.
(33) Majumdar, A.; et al. Chemical synthesis and surface morphology of amorphous hydrogenated carbon nitride film deposited by N2/CH4 dielectric barrier discharge plasma. *Compos. Interfaces* **2012**, *19* (3−4), 161−170.
(34) Trilleras, J.; et al. Computational and Experimental Study on Molecular Structure of Benzo [g] pyrimido 4, 5-b] quinoline Derivatives: Preference of Linear over the Angular Isomer. *Appl. Sci.* **2017**, *7* (10), 967.
(35) Singh, J.; et al. Biogenic ZnO nanoparticles: A study of blueshift of optical band gap and photocatalytic degradation of reactive yellow 186 dye under direct sunlight. *Green Process. Synth.* **2019**, *8* (1), 272−280.
(36) Yashwanth, H. J.; Rondiya, S. R.; Eya, H. I.; Dzade, N. Z.; Phase, D. M.; Dhole, S. D.; Hareesh, K. Synergy between nitrogen, phosphorus co-doped carbon quantum dots and ZnO nanorods for enhanced hydrogen production. *J. Alloys Compd.* **2023**, *937*, 168397.
(37) Saha, S.; et al. Graphene Quantum Dots as Hole Extraction and Transfer Layer Empowering Solar Water Splitting of Catalyst-Coupled Zinc Ferrite Nanorods. *ACS Appl. Mater. Interfaces* **2024**, *16* (22), 28441−28451.
(38) Han, B.; et al. A high response butanol gas sensor based on ZnO hollow spheres. *Sens. Actuators, B* **2016**, *237*, 423−430.
(39) Yang, X.; et al. Nitrogen-doped ZnO nanowire arrays for photoelectrochemical water splitting. *Nano Lett.* **2009**, *9* (6), 2331−2336.
(40) Yu, W.; Xu, D.; Peng, T. Enhanced photocatalytic activity of gC 3 N 4 for selective CO 2 reduction to CH 3 OH via facile coupling of ZnO: A direct Z-scheme mechanism. *J. Mater. Chem. A* **2015**, *3* (39), 19936−19947.
(41) El-Hnayn, R.; et al. One-step synthesis of diamine-functionalized graphene quantum dots from graphene oxide and their chelating and antioxidant activities. *Nanomaterials* **2020**, *10* (1), 104.
(42) Kehrer, M.; Duchoslav, J.; Hinterreiter, A.; Cobet, M.; Mehic, A.; Stehrer, T.; Stifter, D. XPS investigation on the reactivity of surface imine groups with TFAA. *Plasma Processes Polym.* **2019**, *16* (4), 1800160.
(43) Jung, Y.; et al. High performance and high stability low temperature aqueous solution-derived Li−Zr co-doped ZnO thin film transistors. *J. Mater. Chem.* **2012**, *22* (12), 5390−5397.
(44) Makuła, P.; Pacia, M.; Macyk, W. *How to correctly determine the band gap energy of modified semiconductor photocatalysts based on UV−Vis spectra*. ACS Publications: 2018; pp. 68146817.
(45) Wang, L.; Tan, H.; Zhang, L.; Cheng, B.; Yu, J.; et al. In-situ growth of few-layer graphene on ZnO with intimate interfacial contact for enhanced photocatalytic CO2 reduction activity. *Chem. Eng. J.* **2021**, *411*, 128501.
(46) Ren, H., et al. *Carbon quantum dots modified Z. and S−Scheme heterojunctions for pharmaceutical contaminants photodegradation: state−of−the−art, benefits, and limitations*. Separation and Purification Technology, 2024.
(47) Zhang, B.; et al. Insight into bay-/end-substituted perylene diimide and its S-scheme heterojunction for enhanced photocatalytic H2O2 production under visible-light irradiation. *J. Mater. Sci. Technol.* **2025**, *206*, 257−268.
(48) Tayyebi, A.; et al. ZnO quantum dots-graphene composites: Formation mechanism and enhanced photocatalytic activity for degradation of methyl orange dye. *J. Alloys Compd.* **2016**, *663*, 738−749.
(49) Ansari, S. A.; et al. Oxygen vacancy induced band gap narrowing of ZnO nanostructures by an electrochemically active biofilm. *Nanoscale* **2013**, *5* (19), 9238−9246.
(50) Qu, Y.; Xu, X.; Huang, R.; Qi, W.; Su, R.; He, Z.; et al. Enhanced photocatalytic degradation of antibiotics in water over functionalized N,S-doped carbon quantum dots embedded ZnO nanoflowers under sunlight irradiation. *Chem. Eng. J.* **2020**, *382*, 123016.
(51) Li, Y.; Liu, T.; Feng, S.; Yang, W.; Zhu, Y.; Zhao, Y.; Liu, Z.; Yang, H.; Fu, W.; et al. Au/CdS Core-Shell Sensitized Actinomorphic Flower-Like ZnO Nanorods for Enhanced Photocatalytic Water Splitting Performance. *Nanomaterials* **2021**, *11* (1), 233.
(52) Ahmad, I.; et al. Lu modified ZnO/CNTs composite: A promising photocatalyst for hydrogen evolution under visible light illumination. *J. Colloid Interface Sci.* **2021**, *584*, 182−192.
(53) Gotipamul, P.; Maheswaran, R.; Pandiaraj, S.; Alqarni, S. A.; Chidambaram, S. Piezo-photocatalytically enhanced H2 production and pollutant removal from ZnO nanorods grown on g-C3N4 layers. *Mater. Today. Sustainability* **2023**, *24*, 100501.
(54) Kim, D.; Yong, K. Boron doping induced charge transfer switching of a C3N4/ZnO photocatalyst from Z-scheme to type II to enhance photocatalytic hydrogen production. *Appl. Catal., B* **2021**, *282*, 119538.
(55) Wang, S.; et al. Direct Z-scheme ZnO/CdS hierarchical photocatalyst for enhanced photocatalytic H2-production activity. *Appl. Catal., B* **2019**, *243*, 19−26.
(56) Duan, Y.; Xue, J.; Dai, J.; Wei, Y.; Wu, C.; Chang, S.-H.; Ma, J. Interface engineering of ZnO/In2O3 Z-scheme heterojunction with yolk-shell structure for efficient photocatalytic hydrogen evolution. *Appl. Surf. Sci.* **2022**, *592*, 153306.
(57) Qu, D.; et al. Three Colors Emission from S,N Co-doped Graphene Quantum Dots for Visible Light H2 Production and Bioimaging. *Adv. Opt. Mater.* **2015**, *3* (3), 360−367.
(58) Yang, J.; Miao, H.; Jing, J.; Zhu, Y.; Choi, W.; et al. Photocatalytic activity enhancement of PDI supermolecular via π-π action and energy level adjusting with graphene quantum dots. *Appl. Catal., B* **2021**, *281*, 119547.

https://doi.org/10.1021/acsomega.4c05574
ACS Omega 2024, 9, 40790−40800

(59) Kumar Nahak, B.; Tseng, F. G. Synergistic enhancement of seawater hydrogen generation via sulfur vacancy enriched and phases engineered CQD loaded CdS photocatalyst. *Mater. Adv.* **2024**, *5* (3), 1284−1300.
(60) Zhang, H.; et al. Fast photogenerated electron transfer in N-GQDs/PTI/ZnO-QDs ternary heterostructured nanosheets for photocatalytic H2 evolution under visible light. *Appl. Surf. Sci.* **2019**, *485*, 361−367.
(61) Xu, X., et al. *Surface states engineering carbon dots as multi-band light active sensitizers for ZnO nanowire array photoanode to boost solar water splitting* Elsevier: Carbon, 2017; Vol. *121*; pp. 201208.

https://doi.org/10.1021/acsomega.4c05574
ACS Omega 2024, 9, 40790−40800